ACS OMEGA

Article

Cite This: ACS Omega 2018, 3, 11300−11306

http://pubs.acs.org/journal/acsodf

Synthesis and Phase Transformation Studies of Dysprosium-Doped $Bi_4V_2O_{11}$ Nanoparticles and Their Application in Visible Light Photocatalytic Degradation of Tetracycline Drug

Faria K. Naqvi,[†,§] Mohd. Faraz,[‡,§] Saba Beg,*[,†] and Neeraj Khare[‡]

[†]Department of Chemistry, Aligarh Muslim University, Aligarh 202002, India

[‡]Department of Physic, Indian Institute of Technology Delhi, Delhi 110016, India

Supporting Information

ABSTRACT: Recently, $Bi_4V_2O_{11}$ as an electrolyte material has pulled in considerable consideration because of its remarkable novel applications. In this article, novel, dysprosium-doped (x = 0.2, 0.3, 0.4, and 0.5) $Bi_4V_2O_{11}$ (Dy/BVO) nanoparticles have been synthesized by sol−gel strategy. The photocatalyst Dy/BVO nanoparticles exhibit higher photocatalytic efficiency than BVO nanoparticles assessed by debasement of tetracycline drug under visible light illumination. Our work focuses on the phase transformation, conducting properties, and mechanisms of the Dy/BVO nanoparticles in relation to execute some methods of processing and manufacturing product in commercial applications. The characterization of Dy/BVO was performed by Fourier transform infrared, X-ray diffraction, scanning electron microscopy, energy-dispersive X-ray analysis, and UV−vis analysis. ac impedance spectroscopy was used to analyze the conducting behavior of synthesized nanoparticles in the temperature range 100−600 °C. The photocatalytic activity revealed that Dy/BVO remarkably enhanced the photocatalytic activity. This is the first report that Dy/BVO can destroy the drug effluent which is coming from the drug industry and also worried about the human health hazards.

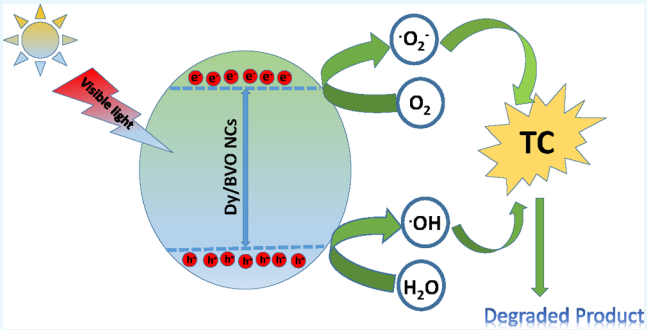

1. INTRODUCTION

Antibiotics are the world's biggest creation and utilization of medications, which play out an imperative part in the avoidance and direction of the malady.[1] Joined by the ascent in the utilization of antibiotics, an extensive number of them are released into the earth including pharmaceutical wastewater and aquaculture wastewater year by year.[2] The presence of pharmaceutical scums in wastewater has pulled in overall consideration because of their ruinous effect on natural issues and human wellbeing through drinking water and evolved way of life.[3] Tetracycline (TC) drug is broadly utilized as a part of different perspectives, for example, bacterial infection,[4] horticulture,[5] and domesticated animal products.[6] It is accounted for that TC sedate is the beside the biggest utilized as a part of the world, representing right around 33% of the anti-infection agents creation and utilization.[7,8] With the unnecessary gathering of antibiotic agents in the human body,[9] they can incite nephropathy, influence kidneys, and different changes, for example, mutagenic and teratogenic impacts.[5] The presence of TC drug in water conditions will influence the structure and action of microorganisms, which subsequently changes the natural structure of the microbial vegetation.[3,10] In order to eliminate the residual antibiotics in ecological water, the current innovation is primarily reliant on activated carbon adsorption,[11] coagulation−flotation,[12] ultrasound degradation, and membrane bioreactor.[11] These strategies are still faced with the trouble of quite a while devouring, vitality utilization, and poor effectiveness. Without a doubt, there is a solid interest for a quick and reasonable technique for the end of antibiotics from sullied water. Among them, photocatalytic degradation is considered as a supportable innovation to evacuate TC drug and the photocatalytic degradation proficiency of TC drug is high.

Bismuth-based oxides, for example, bismuth vanadate (BVO), have pulled in an enormous amount of consideration because of their magnificent properties, for example, protection from corrosion,[13] nontoxic, ferro elasticity,[14] and ionic conductivity.[15] However, the photocatalytic activity of the pure BVO still needs improvement because of its low quantum yield and poor adsorptive execution. This low performance of BVO nanoparticles is due to the difficult passage of photogenerated electron−hole pairs.[14,16] To resolve this problem, doping of metal ion can improve the photocatalytic activity of BVO through separating the photogenerated electrons from holes.[17] Recently, there have been few reports on the advancement of doped BVO to enhance the

Received: May 16, 2018
Accepted: August 28, 2018
Published: September 17, 2018

DOI: 10.1021/acsomega.8b01012
ACS Omega 2018, 3, 11300−11306

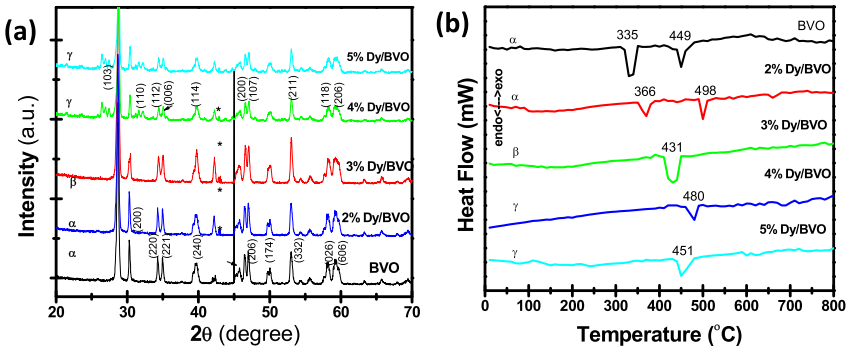

Figure 1. (a) XRD pattern of BVO and Dy-doped BVO nanoparticles. (b) DTA graph of BVO and Dy-doped BVO nanoparticles.

photocatalytic activity under visible light irradiation.[18] In this way, it was thought beneficial to enhance the photocatalytic activity of BVO and the photosensitivity toward visible light utilizing doping agent, for example, Ag,[15] Cu,[14] and C,[19] which have attracted much attention.

Here, in the present study, BVO and dysprosium-doped $Bi_4V_2O_{11}$ (Dy/BVO) nanoparticles were synthesized by the sol−gel technique. The photocatalytic activity of the BVO and Dy/BVO nanoparticles was assessed by the degradation of TC drug under visible light irradiation, and the outcome demonstrated that the Dy/BVO nanoparticles show exceptionally improved photocatalytic activity compared to the BVO nanoparticles.

2. EXPERIMENTAL SECTION

2.1. Materials. All chemicals are used without further purification. The distilled water was used for the whole experimental procedures.

2.2. Synthesis of BVO and Dy/BVO. In the typical synthesis procedure, 1 mol $Bi(NO_3)_3{\cdot}5H_2O$, 1 mol V_2O_5, and required amount of $Dy(NO_3)_3{\cdot}xH_2O$ were dissolved in 100 mL of distilled water, followed by the addition of citric acid in the molar ratio unity. Under constant stirring, ammonia (NH_3) solution was added to maintain the neutrality of the sol. The solution is continuously stirred for few hours while maintaining the temperature of the solution to 60 °C. After a few hours, the color of the solution changes and xerogel is formed. This xerogel is kept at 90 °C. At this temperature, the gel is dried in a self-propagating combustion manner and finally transformed into loose powder. This powder is finally annealed at 600 °C in the open air furnace after grinding.

2.3. Characterization Techniques. A Rigaku Ultima VI X-ray diffractometer with a radiation source of Cu Kα (λ = 1.54 Å) was used to record the X-ray diffraction (XRD) patterns.[12,20] A Carl Zeiss EVO-50 series scanning electron microscope was used to record scanning electron microscopy (SEM) images of BVO and Dy/BVO nanoparticles. The optical properties of the nanoparticles were investigated by a UV−vis diffuse reflectance spectra (PerkinElmer, LAMBDA 1050) spectrophotometer equipped with an integrating sphere.[21] Electrical properties were investigated by ac impedance spectroscopy (Wayne Kerr 4100 LCR meter) operated in the frequency range 1 Hz to 1 MHz.[22] Impedance spectra were subjected to non-linear least-squares fitting using Zview software program.

2.4. Photocatalytic Activity. The application of the BVO and Dy/BVO (x = 0, 0.2, 0.3, 0.4, and 0.5%) nanoparticles to degradation of TC antibiotic drug was evaluated under visible light by using 300 W Xe lamp illumination.[23] In this process, 100 mg of photocatalyst powder was disseminated in 100 mL of the aqueous solution of TC drug with an underlying centralization of 10 mg/L. Before visible light illumination, the subsequent suspension was ultrasonically treated for 15 min and after that stirred in the dark for 1 h to permit the system to establish the adsorption−desorption equilibrium. At given irradiation intervals, 4 mL of the suspension was gathered at specific interims, at that point centrifuged to evacuate the photocatalyst particles, last the solution was separated through a 0.22 μm nylon 66 membrane filter. The filtrate was investigated by recording the maximal absorption of various wavelengths in the UV−vis spectrophotometer.

A control (blank) test was additionally led for the TC solution without Dy/BVO nanoparticles under visible light illumination.

The rate of photodegradation of the photocatalyst can be considered in the accompanying way[24]

$$\%\ \text{degradation} = (1 - C/C_o) \times 100\% \quad (1)$$

where C_o is the concentration of TC drug at adsorption equilibrium and C is the residual concentration of TC drug at different illumination intervals.

The kinetics of photodegradation of TC drug can be articulated as follows[25]

$$\ln(C_o/C) = kt \quad (2)$$

where k (min^{-1}) is the degradation rate constant.

3. RESULTS AND DISCUSSION

The influence of substitution of Dy^{3+} on polymorphism of BVO is shown by XRD patterns at room temperature in Figure 1a. The XRD pattern of BVO shows the stabilization of monoclinic α phase which is confirmed by JCPDS number 82-1481 with a space group symmetry $C2/m$. For 2%, Dy/BVO nanoparticles show a characteristic doublet peak which is observed between 2θ = 46°−46.5° ascribed to (026) and (606) which gives the confirmation of monoclinic α phase. The doublet peak is merged into singlet (220) for 3% Dy/BVO, showing the existence of orthorhombic β-phase. The small peaks (indicated with an asterisk) show the presence of Dy^{3+} incorporated in the BVO lattice. These small peaks were not observed in the pure BVO nanoparticles. Tetragonal γ phase is confirmed (JCPDS number 89-0102) for the 4% Dy/BVO and 5% Dy/BVO nanoparticles at room temperature with a space group symmetry $I4/mmm$. The (200) peaks at 2θ ≈ 31° show the decrement in the sharpness. It is may be because of the incorporation of larger size cation Dy^{3+}

DOI: 10.1021/acsomega.8b01012
ACS Omega 2018, 3, 11300−11306

(0.912A°) in place of smaller cation vanadium (V^{5+} = 0.68A°). Because of this incorporation, the structure of BVO nanoparticles gets disturbed and adapted into more stable phase. Table 1 summarizes the unit cell parameters of various compositions. It is worth mentioning that the unit cell parameters were refined in the mean orthorhombic system, using the space groups, *C*2/*m*, *Aba*2, and *I*4/*mmm* for α, β, and γ phases, respectively. It can be noted that the *c*-parameter generally increases with increasing Dy^{3+} concentration. The average crystallite size of synthesized nanoparticles can be calculated by Debye Scherrer formula,[25a,26,27,27b] and it is near about 80−90 nm.

Table 1. Unit Cell Parameters for Dy^{3+}-Doped BVO ($Bi_4V_2O_{11}$)

composition	*A*	*b*	*c*	*V*	phases
BVO ($Bi_4V_2O_{11}$)	5.522	5.616	15.308	474.724	α
2% Dy BVO	5.522	5.616	15.312	475.003	α
3% Dy BVO	5.541	5.616	15.319	477.687	β
4% Dy BVO	3.963		15.441	241.027	γ
5% Dy BVO	3.967		15.507	241.596	γ

The thermal phase stability of the BVO and Dy/BVO nanoparticles was investigated by differential thermal analysis (DTA) (Figure 1b). On heating, nanoparticles show small double endothermic peaks at 335 and 449 °C for BVO and 2% Dy/BVO nanoparticles, respectively, which are assigned to the α phase, whereas the smaller one single endothermic peak (431 °C) observed in 3% Dy/BVO nanoparticles which are attributed to the $\alpha \rightarrow \beta$ transition. The small endothermic event is associated with oxygen vacancies' order-disorder phase transition which is found in other members of BIMEVOX. The 4% Dy/BVO and 5% Dy/BVO nanoparticles show order → disorder, $\gamma' \rightarrow \gamma$ transition. These transitions are associated with a subtle change that occurs in some oxygen sub lattice positions located in the perovskite-vanadate polyhedral. This assignment is in a good agreement with the results obtained from the XRD analysis.

The morphology of the nanoparticles was analyzed by SEM analysis (Figure 2). Micrographs of BVO and 5% Dy/BVO nanoparticles show the dense morphology with good homogeneity. It is clearly seen in the micrographs that the particles are nonagglomerated and few partially aggregated. The elemental analysis of the nanoparticles was analyzed by energy-dispersive X-ray analysis (EDAX) (Figure 2c,d). The compositions of nanoparticles were confirmed by the inset of the EDAX spectrum. There is no impurity seen in the EDAX spectrum. It is clearly seen in the inset of EDAX that the content of vanadium decreases as the dysprosium doping increases.

The specific surface area and band gap energy of the nanoparticles are shown in Figure 3. The specific surface area of BVO increases on doping with Dy because of the difference in the ionic radii of the dopant and vanadium.[28] Among BVO nanoparticles and Dy/BVO nanoparticles, the BVO has the lowest Brunauer−Emmett−Teller (BET) surface area, whereas doped material 5% Dy/BVO nanoparticles have the highest BET surface area. It is broadly assumed that the catalytic property is mainly determined by the adsorption and desorption of molecules on the surface of the catalyst. The high specific surface area can provide more reactive

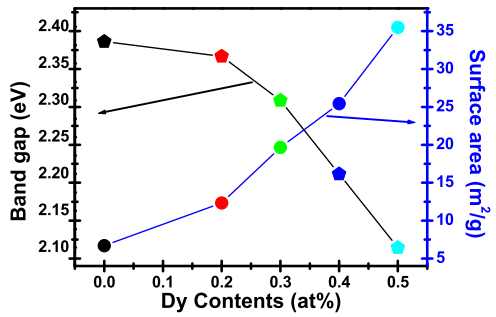

Figure 3. Band gap energy and surface area of BVO and Dy/BVO nanoparticles.

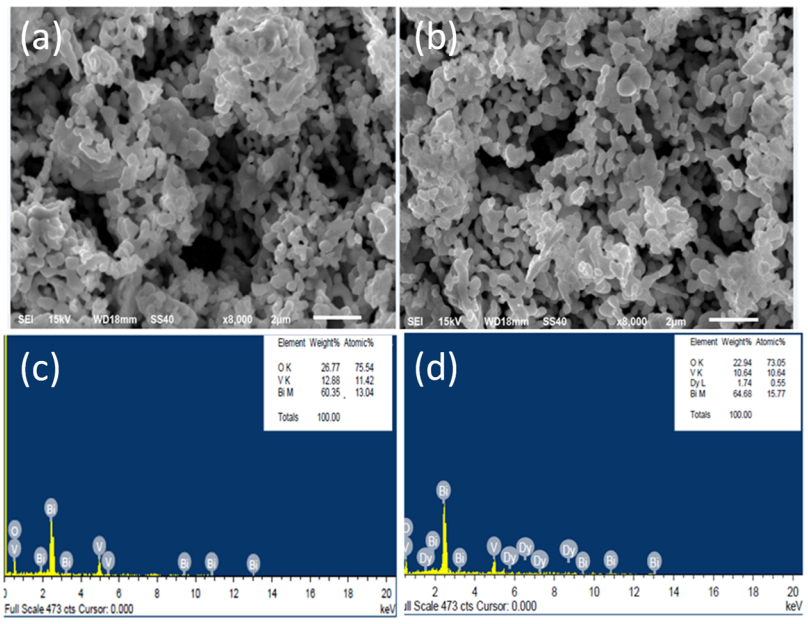

Figure 2. SEM analysis of (a) BVO and (b) 5% Dy/BVO nanoparticles; EDAX analysis of (c) BVO and (d) 5% Dy/BVO nanoparticles.

DOI: 10.1021/acsomega.8b01012
ACS Omega 2018, 3, 11300−11306

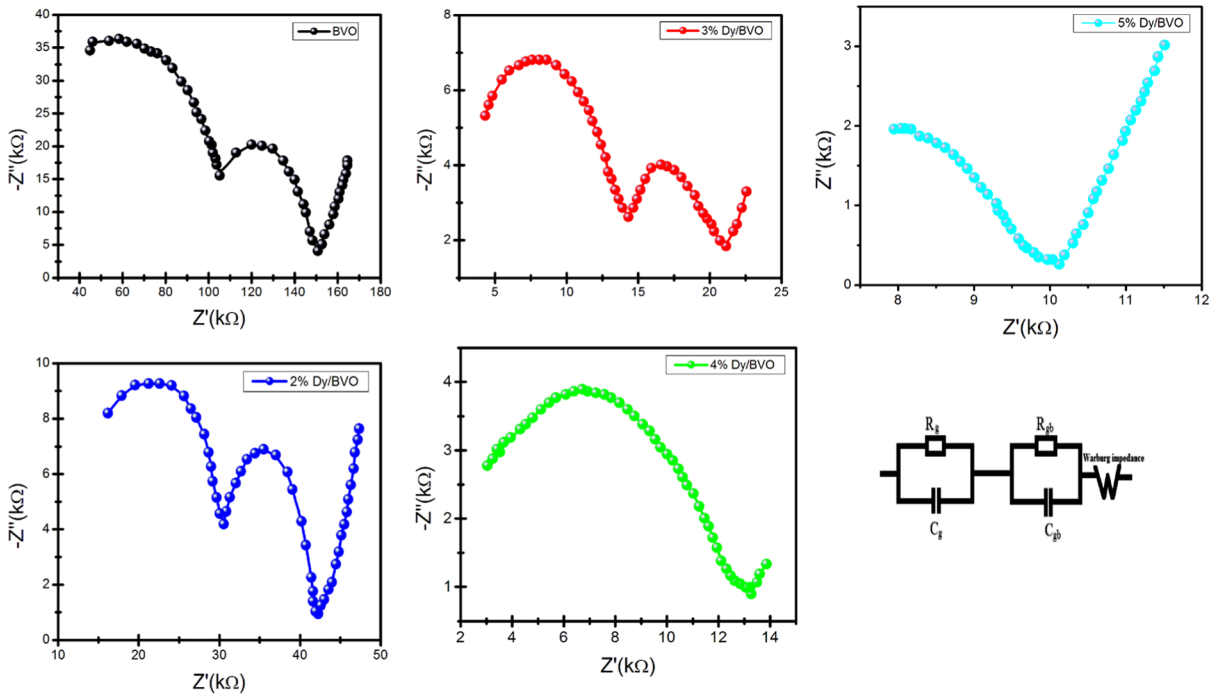

Figure 4. Nyquist plots for BVO and Dy/BVO nanoparticles.

Table 2. Equivalent Circuit Parameters Estimated from the Nyquist Plots for the Different Compositions of Dy/BVO

composition x	R_g	R_{gb}	R_t	ω_g	ω_{gb}	τ_g	τ_{gb}	C_g	C_{gb}
BVO	60.23	46.13	106.36	228.27	127.73	04.38×10^{-3}	07.8×10^{-3}	263.80×10^{-3}	359.81×10^{-3}
2% Dy/BVO	14.46	11.74	26.20	58.71	43.77	17.03×10^{-3}	22.84×10^{-3}	246.45×10^{-3}	268.14×10^{-3}
3% Dy/BVO	10.14	06.67	16.81	42.89	25.24	23.31×10^{-3}	39.61×10^{-3}	236.36×10^{-3}	264.19×10^{-3}
4% Dy/BVO	10.30		10.30	24.42		40.95×10^{-3}		421.78×10^{-3}	
5% Dy/BVO	02.16		2.16	12.24		81.69×10^{-3}		176.45×10^{-3}	

adsorption−desorption sites for photocatalytic reaction.[28] The energy band gap of BVO and Dy/BVO nanoparticles is shown in Figure 3. A slightly lower value of band gap was observed after doping with Dy. The red shift indicated narrowing of the band gap of Dy/BVO nanoparticles which may originate from the charge transfer between the BVO and Dy/BVO valence or conduction band and the Dy ions.

The ac impedance measurements for Dy/BVO (x = 0.0, 0.20, 0.30, 0.40, and 0.50%) nanoparticles are shown in Figure 4. The temperature range between 100 and 600 °C. The single substitution in BVO lattice results in various impedance regimes. As shown in Figure 4, two depressed semicircles at low concentration of Dy^{3+} (3% Dy/BVO) indicate the grain and grain boundary resistances, whereas at higher concentrations of Dy^{3+}, 4% Dy/BVO and 5% Dy/BVO nanoparticles can be attributed to the combination of both grain and grain boundary. The inclined spike appears at low-frequency regions in all of the compositions. This is due to the electrode−electrolyte interface.[29]

The impedance spectra and grain bulk/boundary contribution have been evaluated by two parallel R-CPE elements connected in series with electrolyte resistance shown in Figure 4.

Table 2 represents the values of equivalent circuit parameters for both grain and grain boundary contribution estimated from the impedance plane plots for temperature 300 °C at four different concentrations (x = 0, 0.2, 0.3, 0.4, and 0.5). It can be found that the grain contribution to the oxygen-ionic conductivity is more pronounced than that of the grain boundary contribution because the values of R_g are higher than R_{gb}. It can also be noticed that the reduction in R_g values is faster than R_{gb} with increasing temperature. Moreover, the values of C_{gb} are higher than that of C_g which suggests that the permittivity increases with the accumulation of charge carriers at the grain boundary. The highest values of capacitances C_g are found to be 421.78×10^{-3} at 300 °C for composition 4% Dy/BVO nanoparticles, suggesting more polarizability of the sample at this temperature. Hence, the total electrical permittivity of the sample is mainly attributed to the increased charge accumulation at the grain boundaries. The calculated resistance and conductivity according to the equation ($\sigma = 1/R$) for different compositions (x = 0, 0.2, 0.3, 0.4, and 0.5) at 300 °C are given in Table 3. Highest conductivity is observed for 5% Dy/BVO nanoparticles of about 2.91×10^{-2} S cm^{-1}.

Table 3. Resistance and Conductivity Calculated from Impedance Data of Different Compositions Dy/BVO at 300 °C

s. no.	composition	resistivity (Ω)	conductivity (S cm^{-1})
1.	BVO	106.36	6.77×10^{-4}
2.	2% Dy/BVO	26.2	2.41×10^{-3}
3.	3% Dy/BVO	16.81	3.75×10^{-3}
4.	4% Dy/BVO	10.30	6.12×10^{-3}
5.	5% Dy/BVO	2.16	2.91×10^{-2}

DOI: 10.1021/acsomega.8b01012
ACS Omega 2018, 3, 11300−11306

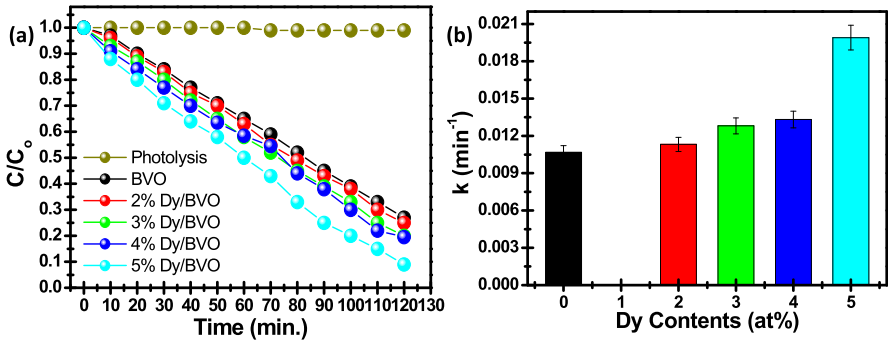

Figure 5. (a) Photodegradation efficiency of TC in the presence of BVO and Dy-doped BVO nanoparticles and (b) pseudo-first-order kinetic rate constant k for TC degradation.

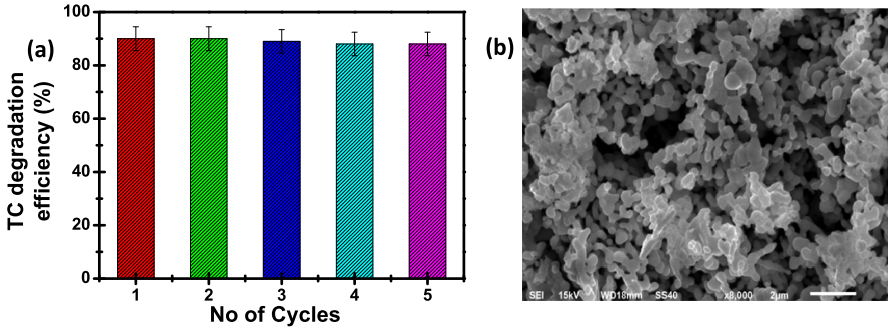

Figure 6. (a) Recycling properties of the 5% Dy/BVO nanocomposites and (b) SEM images of 5% Dy/BVO nanocomposites after the photocatalytic reaction.

3.1. Photocatalytic Activity of the Dy-Doped BVO. Photocatalytic activities of the as-prepared BVO and Dy-doped (2, 3, 4, and 5%) BVO nanoparticles were estimated using TC drug degradation under visible light using Xe lamp irradiation, and the photodegradation efficiency of TC versus reaction time is shown in Figure 5a. Because of the stability of TC drug, the degradation TC drug were very low in the absence of the photocatalyst under dark and visible light irradiation. In the case of BVO nanoparticle photocatalysts, only 3% of TC is removed within 60 min without light irradiation. However, under the same conditions, about 5% of TC is absorbed by Dy/BVO photocatalysts, which is due to the fact that drug molecules can adsorb from solution to the surface of photocatalysts. The comparative study of photodegradation of TC drug over different Dy/BVO as a photocatalyst for a period of 120 min in the photoreactor has been carried out. It has been noticed that Dy/BVO nanoparticles exhibit higher photocatalytic activity as compared with BVO nanoparticles. To know the reaction kinetics of TC drug degradation in this study, the pseudo-first-order kinetics equation is used to fit experimental data. The degradation of TC follows pseudo-first-order reaction kinetics. The values are present in Figure 5b.

3.1.1. Recycle and Stability of the Catalyst. The reusability of the photocatalytic is a serious problem for long-term use in the realistic application of the photocatalyst. The reusability of Dy/BVO nanoparticles was tested for the degradation of TC under identical reaction conditions. After complete degradation, the catalysts were separated and washed with deionized water. The recovered catalysts were dried and used for the next run. Figure 6a shows the results of TC drug photodegradation for five runs of the 5% Dy/BVO nanoparticles. 5% Dy/BVO nanoparticles exhibit TC drug degradation efficiency which is 95−93% from first to fifth runs, respectively, for 120 min. Furthermore, 5% Dy/BVO nanoparticles can be easily separated when compared to the BVO nanoparticles. Figure 6b shows SEM image of 5% Dy/BVO nanoparticles after the fifth run.

3.1.2. Active Species Responsible for TC Degradation. To elucidate the photocatalytic mechanism, *tert*-butyl alcohol (TBA, a hydroxyl radical scavenge) and disodium salt of ethlyenediaminetetraacetic acid (EDTA-2Na, a photogenerated hole scavenger) were adopted as a scavenger in the reaction system of TC drug degradation over Dy/BVO nanoparticles. Figure 7 shows that the degradation of TC drug rate does show an obvious change in the presence of TBA and EDTA-2Na, indicating that h^+ and $^{\bullet}OH$ are main reactive species in the photocatalyst reaction.

3.2. Enhanced Photocatalytic Degradation Mechanism of TC Drug on Dy/BVO. The mechanism involved in

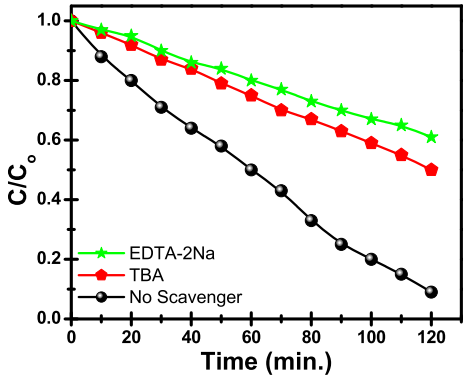

Figure 7. Effect of different scavengers on the degradation of TC drug in the presence of 5% Dy/BVO nanoparticles.

DOI: 10.1021/acsomega.8b01012
ACS Omega 2018, 3, 11300−11306

the photocatalytic degradation of BVO and Dy-doped BVO nanoparticles has been diagrammatically represented in Figure 8. The band gap of synthesized BVO, 2% Dy/BVO, 3% Dy/BVO, 4% Dy/BVO, and 5% Dy/BVO nanoparticles was found to be 2.36, 2.30, 2.20, and 2.10 eV lower than the BVO 2.38 eV, respectively. Photocatalytic reaction occurs due to the excitation of a photoelectron from filled valence band of Dy/BVO nanoparticles to the empty conduction band by the irradiation of visible light energy ($h\nu$) either equal to or greater than the band gap Dy/BVO nanoparticles which results in the creation of a hole (h^+) in the valence band. The overall result is the formation of the electron (e^-) and hole pairs which act as an oxidizing and reducing agent, respectively.[30]

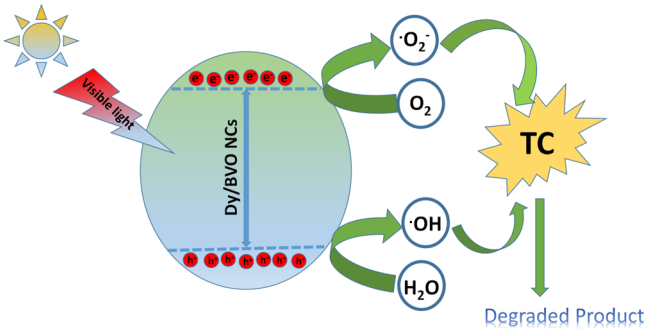

Figure 8. Proposed reaction mechanism for the photocatalytic degradation of TC using 5% Dy/BVO nanoparticles under visible light.

The nonradiative recombination of electron and hole pairs is due to the higher band gap of the nanoparticles which leads to initiate the photocatalytic activity of TC drug. Hydroxyl radical ($HO^\bullet$) gets oxidized by the water, which is adsorbed on the surface of 5% Dy/BVO nanoparticles. Subsequently, from the conduction band, the electrons were taken up by oxygen. Now that oxygen radical converted into an anionic superoxide radical which not only takes part in the further oxidation process but also prevents the electron−hole recombination, maintaining the electron neutrality within the 5% Dy/BVO nanoparticles. The superoxide recombines with a proton to give ($HOO^\bullet$) which ultimately generate H_2O_2 which further dissociates into highly reactive hydroxyl radicals ($HO^\bullet$) which can further oxidize TC.

$$\text{Dy/BVO} + h\nu \rightarrow e^- + h^+$$

$$H_2O_2 + e^- \rightarrow HO^- + HO^\bullet$$

$$H_2O_2 + HO^\bullet \rightarrow HOO^\bullet + H_2O$$

$$HOO^\bullet + HO^\bullet \rightarrow H_2O + O_2$$

$$H_2O_2 + h^+ \rightarrow O_2 + 2H^+$$

$$h^+ + O_2 + \text{TC drug} \rightarrow CO_2 + H_2O \text{ (degraded product)}$$

4. CONCLUSIONS

The BVO and Dy-doped BVO nanoparticles were successfully synthesized by the sol−gel method. These nanoparticles were characterized by various analytical techniques such as XRD, UV−vis, SEM, photoluminescence, and EDAX spectroscopy. It is observed that the high conducting γ phase is stabilized for the compositions 4% Dy/BVO and 5% Dy/BVO nanoparticles. The highest conductivity is observed for sample 5% Dy/BVO which is 2.91×10^{-2} S cm^{-1} at 300 °C. The photodegradation of the TC under visible light irradiation by BVO and Dy-doped BVO nanoparticles has been done, and it has been observed that the highest photocatalytic was shown by 5% Dy/BVO as compared to the other BVO nanoparticles.

■ ASSOCIATED CONTENT

Supporting Information

The Supporting Information is available free of charge on the ACS Publications website at DOI: 10.1021/acsomega.8b01012.

Photodegradation efficiency of TC in the absence of 5% Dy-doped BVO nanoparticles and UV−vis spectra of Dy/BVO nanoparticles (PDF)

■ AUTHOR INFORMATION

Corresponding Author

*E-mail: profsababeg@gmail.com.

ORCID

Saba Beg: 0000-0002-7781-1747

Author Contributions

§F.K.N. and M.F. contributed equally.

Notes

The authors declare no competing financial interest.

■ ACKNOWLEDGMENTS

This work is supported by the department of science and technology, India (PDF/2017/002797). We would also like to express our sincere gratitude to UGC.

■ REFERENCES

(1) WHO. *Scaling up the Response To Infectious Diseases: A Way Out of Poverty: Report on Infectious Diseases 2002*, 2002.

(2) Gaw, S.; Thomas, K. V.; Hutchinson, T. H. Sources, impacts and trends of pharmaceuticals in the marine and coastal environment. *Philos. Trans. R. Soc., B* **2014**, *369*, 20130572.

(3) Deng, F.; Zhao, L.; Luo, X.; Luo, S.; Dionysiou, D. D. Highly efficient visible-light photocatalytic performance of Ag/AgIn 5 S 8 for degradation of tetracycline hydrochloride and treatment of real pharmaceutical industry wastewater. *Chem. Eng. J.* **2018**, *333*, 423−433.

(4) Chopra, I.; Roberts, M. Tetracycline antibiotics: mode of action, applications, molecular biology, and epidemiology of bacterial resistance. *Microbiol. Mol. Biol. Rev.* **2001**, *65*, 232−260.

(5) Wang, D.; Jia, F.; Wang, H.; Chen, F.; Fang, Y.; Dong, W.; Zeng, G.; Li, X.; Yang, Q.; Yuan, X. Simultaneously efficient adsorption and photocatalytic degradation of tetracycline by Fe-based MOFs. *J. Colloid Interface Sci.* **2018**, *519*, 273−284.

(6) Hardt, W.-D.; Kaiser, P.; Sirard, J.-C.; Carnoy, C.; Fougeron, D.; Chabalgoity, J. A.; Munoz, N. Methods and pharmaceutical compositions for the treatment of bacterial infections. Google Patents, WO2015011254A1, Application 29 Jan **2015**.

(7) Artigas, A.; Carlet, J.; Martin-Loeches, I.; Niederman, M.; Torres, A. 23rd International Symposium on Infections in the Critically Ill Patient. *Med. Sci.* **2018**, *6*, 13.

(8) Granados-Chinchilla, F.; Rodríguez, C. Tetracyclines in Food and Feedingstuffs: From Regulation to Analytical Methods, Bacterial Resistance, and Environmental and Health Implications. *J. Anal. Methods Chem.* **2017**, *2017*, 1−24.

(9) Guo, J.; Zhou, H.; Wang, J.; Liu, W.; Cheng, M.; Peng, X.; Qin, H.; Wei, J.; Jin, P.; Li, J.; Zhang, X. Nano vanadium dioxide films deposited on biomedical titanium: a novel approach for simulta-

DOI: 10.1021/acsomega.8b01012
ACS Omega 2018, 3, 11300−11306

neously enhanced osteogenic and antibacterial effects. *Artif. Cells, Nanomed., Biotechnol.* **2018**, *21*, 1−17.
(10) Kummerer, K. Resistance in the environment. *J. Antimicrob. Chemother.* **2004**, *54*, 311−320.
(11) Varjani, S. J.; Sudha, M. C. Treatment Technologies for Emerging Organic Contaminants Removal from Wastewater. *Water Remediation*; Springer, 2018; pp 91−115.
(12) Singh, H. H.; Khare, N. Flexible ZnO-PVDF/PTFE Based Piezo-Tribo Hybrid Nanogenerator. *Nano Energy* **2018**, *51*, 216−222.
(13) Kant, R. Studies of Some Bismuth Based Electrolytes For Solid Oxide Fuel Cells. Ph.D. Thesis, Thapar University, 2008.
(14) Gao, X.-M.; Fu, F.; Li, W.-H. Photocatalytic degradation of phenol over Cu loading BiVO4 metal composite oxides under visible light irradiation. *Phys. B* **2013**, *412*, 26−31.
(15) Xue, Y.; Wang, X. The effects of Ag doping on crystalline structure and photocatalytic properties of BiVO4. *Int. J. Hydrogen Energy* **2015**, *40*, 5878−5888.
(16) Ke, D.; Peng, T.; Ma, L.; Cai, P.; Dai, K. Effects of Hydrothermal Temperature on the Microstructures of BiVO4and Its Photocatalytic O2Evolution Activity under Visible Light. *Inorg. Chem.* **2009**, *48*, 4685−4691.
(17) Cai, P.; Zhou, S.-M.; Ma, D.-K.; Liu, S.-N.; Chen, W.; Huang, S.-M. Fe2O3-Modified Porous BiVO4 Nanoplates with Enhanced Photocatalytic Activity. *Nano-Micro Lett.* **2015**, *7*, 183−193.
(18) (a) Ge, L. Novel visible-light-driven Pt/BiVO4 photocatalyst for efficient degradation of methyl orange. *J. Mol. Catal. A: Chem.* **2008**, *282*, 62−66. (b) Ge, L. Novel visible-light-driven Pt/BiVO4 photocatalyst for efficient degradation of methyl orange. *J. Mol. Catal. A: Chem.* **2008**, *282*, 62−66. (c) Zhou, B.; Zhao, X.; Liu, H.; Qu, J.; Huang, C. P. Visible-light sensitive cobalt-doped BiVO4 (Co-BiVO4) photocatalytic composites for the degradation of methylene blue dye in dilute aqueous solutions. *Appl. Catal., B* **2010**, *99*, 214−221.
(19) Zeng, J.; Zhong, J.; Li, J.; Huang, S. Fabrication of Dy-doped BiVO4with Enhanced Solar Light Photocatalytic Performance. *Synth. React. Inorg., Met.-Org., Nano-Met. Chem.* **2014**, *45*, 476−481.
(20) Momeni, M. M.; Ghayeb, Y.; Davarzadeh, M. WO3nanoparticles anchored on titania nanotube films as efficient photoanodes. *Surf. Eng.* **2015**, *31*, 259−264.
(21) Sohail, A.; Faraz, M.; Arif, H.; Bhat, S. A.; Siddiqui, A. A.; Bano, B. Deciphering the interaction of bovine heart cystatin with ZnO nanoparticles: Spectroscopic and thermodynamic approach. *Int. J. Biol. Macromol.* **2017**, *95*, 1056−1063.
(22) Poornaprakash, B.; Amaranatha Reddy, D.; Murali, G.; Madhusudhana Rao, N.; Vijayalakshmi, R. P.; Reddy, B. K. Composition dependent room temperature ferromagnetism and PL intensity of cobalt doped ZnS nanoparticles. *J. Alloys Compd.* **2013**, *577*, 79−85.
(23) Shakir, M.; Faraz, M.; Sherwani, M. A.; Al-Resayes, S. I. Photocatalytic degradation of the Paracetamol drug using Lanthanum doped ZnO nanoparticles and their in-vitro cytotoxicity assay. *J. Lumin.* **2016**, *176*, 159−167.
(24) Shakir, M.; Faraz, M.; Shoeb Khan, M.; Al-Resayes, S. I. The photocatalytic, in vitro anthelmintic activity of biomolecule-inspired CDS nanoparticles. *C. R. Chim.* **2015**, *18*, 966−978.
(25) (a) Faraz, M.; Naqvi, F. K.; Shakir, M.; Khare, N. Synthesis of samarium-doped zinc oxide nanoparticles with improved photocatalytic performance and recyclability under visible light irradiation. *New J. Chem.* **2018**, *42*, 2295−2305. (b) Ansari, M. Z.; Faraz, M.; Munjal, S.; Kumar, V.; Khare, N. Highly dispersible and uniform size Cu 2 ZnSnS 4 nanoparticles for photocatalytic application. *Adv. Powder Technol.* **2017**, *28*, 2402−2409.
(26) Faraz, M.; Shakir, M.; Khare, N. Highly sensitive and selective detection of picric acid using a one pot biomolecule inspired polyindole/CdS nanocomposite. *New J. Chem.* **2017**, *41*, 5784−5793.
(27) (a) Faraz, M.; Abbasi, A.; Naqvi, F. K.; Khare, N.; Prasad, R.; Barman, I.; Pandey, R. Polyindole/cadmium sulphide nanocomposite based turn-on, multi-ion fluorescence sensor for detection of Cr 3+ , Fe 3+ and Sn 2+ ions. *Sens. Actuators, B* **2018**, *269*, 195−202. (b) Faraz, M.; Ansari, M. Z.; Khare, N. Synthesis of nanostructure manganese doped zinc oxide/polystyrene thin films with excellent stability, transparency and super-hydrophobicity. *Mater. Chem. Phys.* **2018**, *211*, 137−143.
(28) Zeng, J.; Zhong, J.; Li, J.; Huang, S. Fabrication of Dy-doped BiVO4with Enhanced Solar Light Photocatalytic Performance. *Synth. React. Inorg., Met.-Org., Nano-Met. Chem.* **2015**, *45*, 476−481.
(29) Khatoon, N.F.; Saba, B.; S, A.-A. N. A. AC impedance and cyclic voltammetric investigations on BIPBVOX solid electrolyte. *Emerging Mater. Res.* **2017**, *6*, 348−355.
(30) Sharma, S.; Singh, S.; Khare, N. Enhanced photosensitization of zinc oxide nanorods using polyaniline for efficient photocatalytic and photoelectrochemical water splitting. *Int. J. Hydrogen Energy* **2016**, *41*, 21088−21098.

DOI: 10.1021/acsomega.8b01012
ACS Omega 2018, 3, 11300−11306